DIFFRACTION OF HORIZONTALLY POLARIZED SHEAR WAVES BY NORMAL EDGE CRACKS IN A PLATE

Z. Abduljabbar and S.K. Datta

Department of Mechanical Engineering
University of Colorado
Boulder, CO 80309

ABSTRACT

A combined finite element and analytical method is presented here for analyzing scattering of time harmonic horizontally polarized shear (SH) waves by material and geometric irregularities in an isotropic linearly elastic infinite plate. All the irregularities are assumed to be contained in a bounded region. The problem of scattering is solved by replacing this region with a finite element mesh. A nodal force-displacement relation is developed to satisfy the continuity conditions along the boundaries separating the inner finite-element region from the exterior regular region. The method is illustrated by solving the problem of scattering of SH waves by a surface breaking crack. The crack is taken to be normal to the surface of the plate. The reflection and transmission coefficients are computed for zeroth, first, and second incident wave modes. The validity and accuracy of the results are checked by satisfaction of the energy conservation principle and the reciprocity relations.

I. INTRODUCTION

Recently, it has been demonstrated that inspection of long planar cracks in plates can be carried out using horizontally polarized shear (SH) waves generated and detected by electromagnetic-acoustic transducers (EMATs)[1,2]. One major advantage of SH waves over SV, L, and surface waves is that there is no mode conversion when the polarization is along the long defect dimension. An SH wave EMAT technique that is particularly well suited for detection and dimensioning of planar defects in butt weldments has recently been documented.[3] The present theoretical study on diffraction of

SH waves by a normal edge crack in a plate has been motivated by these experimental findings.

Although the subject of diffraction of elastic waves by cracks and inhomogeneities in an infinite medium has been well studied in the past, only recently has attention been paid on diffraction of elastic waves in a bounded medium. Among these are the studies on diffraction by normal edge and buried cracks in a semi-infinite medium.[4-7] A numerical technique based on an integral equation formulation was used in these works. Diffraction of SH waves by an edge crack with arbitrary orientation was studied analytically[8] by a method of matched asymptotic expansions. The techniques used in these works have their limitations, which become quite severe if the crack is located in a region of different material properties (like a weld) from the surrounding homogeneous medium.

Recently,[9-11] a technique combining an analytical procedure with a finite element method has been used to study the diffraction of SH waves by cracks and cavities located either at the surface or at a depth in a semi-infinite medium. The technique has the advantage that the inhomogeneities can be quite arbitrary in shape and material properties. Also, diffraction by a cluster of inhomogeneities can be analyzed. In this method the crack (or inhomogeneity) and the surrounding inhomogeneous material (if necessary) are enclosed completely by a contour. The region interior to the contour is bounded and is represented by finite elements. Wave function expansions are used in the region outside the contour. Continuity conditions for the displacement and traction are imposed at the contour.

The problem of diffraction of elastic waves in a plate is even more complex and only a few solutions are available. One of these is a finite element method[12] which was developed for the study of structural response to SH waves. In this the whole plate is divided into finite and semi-infinite elements and the problem is solved in terms of approximate SH modes. This is not very useful for the calculation of reflection and transmission coefficients of exact SH modes. Another technique[13] is based on the method of the Riemann-Hilbert problem and is not extendable to more complex scattering geometries.

In the present paper a combined finite element and analytical technique is presented for studying diffraction of SH waves in a linearly elastic isotropic homogeneous plate. In this approach the plate is modeled by two rectangular semi-infinite uniform regions separated by a bounded region, which contains all the inhomogeneities (see Fig. 1). The regions are connected along vertical boundaries. The surfaces of the plate are taken to be stress free. To overcome the difficulty in analyzing scattering by arbitrary inhomogeneities lying in the inner region this is divided into finite elements, whereas the solution outside the region is expanded in a modal sum.

The connection between the inner and outer regions is established by finding a set of nodal line forces equivalent to the stress vector acting at the vertical boundaries. These nodal forces are found to be linearly related to the nodal displacements. This leads to the construction of the continuity conditions across these boundaries. The method described above is formulated in its general form and used to study diffraction of SH waves by a normal surface breaking crack in the plate. The reciprocity relations associated with reflection and transmission coefficients are obtained. These relations together with the principle of conservation of energy are used as checks on the numerical results.

II. FORMULATION

The plate considered in the following analysis is assumed to be of uniform thickness h and traction-free surfaces. The material of the plate is taken to be of volume density ρ and shear modulus μ. As shown in Fig. 1 all the inhomogeneities in the plate are contained in region R_2, which is bounded by the vertical lines $x = x_r$, $-x_\ell$. The waves studied here are assumed to be time harmonic SH waves propagating in the x-directions of Fig. 1. The complex time factor $e^{-i\omega t}$, where ω is the circular frequency and t is the time, is

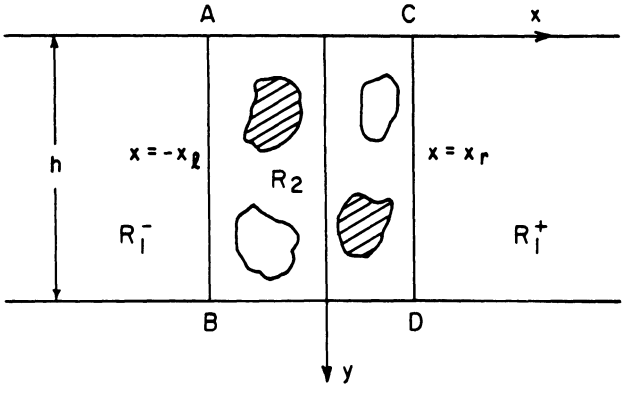

Fig. 1. Typical plate.

factored out in the analysis. In the domain of the plate the z-component of the particle displacement (which is the only non-vanishing component) is given by

$$w = w^i + w^s \quad , \tag{1}$$

where w^i denotes the incident field which is taken as a single shear mode of order m travelling in the positive x-direction of Fig. 1. w^s denotes the scattered field, which is composed of all the modes (propagating and non-propagating). For the incident wave we can write the expression

$$w^i(x,y) = A_m \cos\beta_m y \, e^{\hat{i}k_m x} \quad , \tag{2}$$

where $k_m = \sqrt{k_s^2 - \beta_m^2}$ is the wave number of the incident mode, $\beta_m = \frac{m\pi}{h}$, $k_s = \omega\sqrt{\rho/\mu}$ is the wave number for shear waves in the material of the plate and $\hat{i} = \sqrt{-1}$.

In the exterior regions R_1^- and R_1^+ the scattered field will be approximated by the superposition of a finite number of normal modes. These are either propagating or decaying in the negative and positive x-directions, respectively. This results in the expressions

$$w^s(x,y) = \sum_{n=0}^{N} B_n \cos\beta_n y \, e^{-\hat{i}k_n x} \quad , \; x \leqq -x_\ell \tag{3a}$$

$$w^s(x,y) = \sum_{n=0}^{N} C_n \cos\beta_n y \, e^{\hat{i}k_n x} \quad , \; x \geqq x_r \quad , \tag{3b}$$

where B_n and C_n are the amplitudes of the n-th mode of the scattered field. The number of modes $N+1$ used in expressions (3) is chosen sufficiently larger than the number of propagating modes which is given by

$$N_p = \left[\frac{k_s h}{\pi} \right]^* + 1 \tag{4}$$

in which $[\chi]^*$ denotes the largest integer in χ.

Region R_2 containing the scatterers is represented by a finite element mesh. In this region the total displacement w is then given by its nodal values and the shape functions associated with the mesh. To arrive at the equations governing w in R_2 the variational principle is used. Isoparametric elements are used in this paper. For each element the mechanical properties relevant to this problem are shear modulus μ_e and density ρ_e. In the domain

of each element the total displacement w is given by

$$w(s,t) = \sum_{i=1}^{M} L_i(s,t)\, w_i \quad , \tag{5}$$

where M is the number of nodes in the element under consideration. In (5), the shape functions L_i are used to obtain the particle displacement w from the nodal displacements w_i in terms of the local coordinates s and t. For isoparametric elements the same interpolation is used to relate the global coordinates x, y to the local coordinates through the element nodal coordinates x_i, y_i. This is given by the equations

$$x(s,t) = \sum_{i=1}^{M} L_i(s,t)\, x_i \tag{6a}$$

$$y(s,t) = \sum_{i=1}^{M} L_i(s,t)\, y_i \quad . \tag{6b}$$

The global derivatives are then given in terms of the derivatives with respect to the local coordinates by the relation

$$\begin{Bmatrix} \dfrac{\partial L_i}{\partial x} \\ \\ \dfrac{\partial L_i}{\partial y} \end{Bmatrix} = J^{-1} \begin{Bmatrix} \dfrac{\partial L_i}{\partial s} \\ \\ \dfrac{\partial L_i}{\partial t} \end{Bmatrix} \quad , \tag{7}$$

where J is the Jacobian matrix given by

$$J = \begin{bmatrix} \dfrac{\partial x}{\partial s} & \dfrac{\partial y}{\partial s} \\ \\ \dfrac{\partial x}{\partial t} & \dfrac{\partial y}{\partial t} \end{bmatrix} \quad . \tag{8}$$

The variational formulation requires the minimization of the functional[14]

$$f = U - \frac{1}{2}\rho_e \omega^2 \iiint_V \bar{w}^T w \, dV - \frac{1}{2} \sum_{i=1}^{M} p_i \bar{w}_i - \frac{1}{2} \sum_{i=1}^{M} \bar{p}_i w_i \quad , \tag{9}$$

where U = strain energy
V = volume of element
p_i = element nodal forces.
The overbar in equation (9) denotes complex conjugate while the superscript T denotes transpose. The strain energy U for the element is given by

$$U = \iiint_V \{\bar{\tau}\}^T \{\varepsilon\} \, dv \tag{10}$$

where $\{\tau\}$ and $\{\varepsilon\}$ are, respectively, the column vectors containing the stresses and strains. These vectors are given by

$$\{\tau\} = \begin{Bmatrix} \tau_{xz} \\ \tau_{yz} \end{Bmatrix} \tag{11a}$$

and

$$\{\varepsilon\} = \begin{Bmatrix} \varepsilon_{xz} \\ \varepsilon_{yz} \end{Bmatrix} \tag{11b}$$

where the strains ε_{xz} and ε_{yz} are given by $\varepsilon_{xz} = \frac{1}{2}\frac{\partial w}{\partial x}$ and $\varepsilon_{yz} = \frac{1}{2}\frac{\partial w}{\partial y}$.

The constitutive relation relating the stresses and strains in a linearly elastic isotropic element is given by

$$\{\tau\} = 2\mu_e \{\varepsilon\} \tag{12}$$

The formulation presented here does not involve any anisotropic elements. However, anisotropic elements can be easily included by using suitable constitutive relations.

Combining expressions (5), (8), (10) and (12) with equation (9) we obtain the desired functional f. The minimization of f implies that

$$\frac{\partial f}{\partial \bar{w}_j} = 0 \ , \quad j = 0 \ , \ \text{---} \ , \ M \tag{13}$$

Using (13) we then obtain the element equation in the form

$$[K]\{w\} = \{p\} \tag{14}$$

in which $\{w\}$ and $\{p\}$ are the column vectors containing the nodal

displacements and forces respectively, whereas [K] is an MxM matrix whose elements are given by

$$K_{ij} = \mu_e \left[\int_{-1}^{1} \int_{-1}^{1} \left[\alpha \frac{\partial L_i}{\partial s} \frac{\partial L_j}{\partial s} + \gamma \left(\frac{\partial L_i}{\partial s} \frac{\partial L_j}{\partial t} + \frac{\partial L_i}{\partial t} \frac{\partial L_j}{\partial s} \right) + \beta \frac{\partial L_i}{\partial t} \frac{\partial L_j}{\partial t} \right] \frac{1}{|J|} \, ds \, dt - K_e^2 \int_{-1}^{1} \int_{-1}^{1} L_i L_j \, |J| \, ds \, dt \right] \tag{15}$$

$$K_e^2 = \frac{\omega^2 \rho_e}{\mu_e}$$

$$\alpha = \left(\frac{\partial x}{\partial t} \right)^2 + \left(\frac{\partial y}{\partial t} \right)^2$$

$$\beta = \left(\frac{\partial x}{\partial s} \right)^2 + \left(\frac{\partial y}{\partial t} \right)^2$$

$$\gamma = - \left(\frac{\partial x}{\partial s} \frac{\partial x}{\partial t} + \frac{\partial y}{\partial s} \frac{\partial y}{\partial t} \right)$$

$|J|$ = determinant of the Jacobian matrix

$$= \frac{\partial x}{\partial s} \frac{\partial y}{\partial t} - \frac{\partial y}{\partial s} \frac{\partial x}{\partial t}$$

K_e can be thought of as the wave number associated with the element under consideration. The integration in equation (15) is performed numerically to complete the derivation of the element equation. The assembly of the element-equations into a global equation is a standard procedure[15] in the finite element method and will not be discussed further. This equation can be written in the form

$$[S] \{w\} = \{F\} \tag{16}$$

where [S] is the global matrix obtained by assembling the matrices of all the elements in the mesh. The column vectors $\{w\}$ and $\{F\}$ contain the nodal displacements and loads respectively. The components of $\{F\}$ are given by

$$F_i = \begin{cases} 0 & \text{if } i \text{ denotes an internal or a surface node,} \\ F_i^- & \text{if } i \text{ denotes a node along AB in Fig. 1,} \\ F_i^+ & \text{if } i \text{ denotes a node along CD in Fig. 1.} \end{cases} \tag{17}$$

Equation (17) represents the nodal forces applied to the mesh which is free of loading except for the forces connecting it to R_1. The next step in the formulation is the derivation of the relations between each of F_i^- and F_i^+ and the nodal displacements along the relevant boundary.

Along the boundaries AB and CD the displacement w^s is given by equations (3) at $x = -x_\ell$ and $x = x_r$. This yields the relations

$$w_j^{s-} = \sum_{n=0}^{N} B_n \cos\beta_n y_j \, e^{\hat{i}k_n x_\ell} \tag{18a}$$

$$w_j^{s+} = \sum_{n=0}^{N} C_n \cos\beta_n y_j \, e^{\hat{i}k_n x_r} \tag{18b}$$

where w_j^{s-} and w_j^{s+} are the values of w^s at the j-th node along the relevant boundary. Equations (18) represent two Fourier series of the discrete type[16,17]. In order to apply the discrete Fourier analysis we have to use a number (N+1) of equally spaced nodes along each of the boundaries AB and CD. This results in

$$y_j = \frac{j}{N} h \ , \ j = 0 \ , \ \text{---} \ , \ N \tag{19}$$

The orthogonality relation relevant to the problem is

$$\sum_{j=0}^{N}{}' \cos\frac{n\pi j}{N} \cos\frac{m\pi j}{N} = \begin{cases} 0 \ , & m \neq n \\ \frac{N}{2} \ , & m = n \neq 0, N \\ N \ , & m = n = 0, N \end{cases} \tag{20}$$

where $\sum'$ implies that both the first and last terms in the summation must be multiplied by 1/2. The proof of equation (20) can be established by mathematical induction. For brevity equations (18) can be written in the form

$$w_j^{s\pm} = \sum_{n=0}^{N}{}' D_n^{\pm} \cos\beta_n y_j \tag{21}$$

where $D_n^- = B_n e^{\hat{i}k_n x_\ell}$ and $D_n^+ = C_n e^{\hat{i}k_n x_r}$. The use of relation (20) with equation (21) yields

$$D_n^{\pm} = \begin{cases} \frac{1}{N} \sum_{j=0}^{N}{}' w_j^{s\pm} \cos\beta_n & n = 0, N \\ \frac{2}{N} \sum_{j=0}^{N}{}' w_j^{s\pm} \cos\beta_n y_j & n \neq 0, N \end{cases} \tag{22}$$

In matrix notation equations (21) and (22) can be written as

$$\{w^{s\pm}\} = [V]\{D^{\pm}\} \tag{23}$$

and

$$\{D^{\pm}\} = \frac{2}{N}[E][V][E]\{w^{s\pm}\} \tag{24}$$

respectively. In (23) and (24) $\{w^{s-}\}$ and $\{w^{s+}\}$ denote the column vectors containing the nodal values of w^s along the boundaries AB and CD, respectively; while the column vectors $\{D^{\pm}\}$ contain the amplitudes $D_n^{\pm}$. Also in (23) and (24) [V] is an (N+1) x (N+1) symmetric matrix whose elements are given by

$$V_{ij} = \cos\beta_i y_j$$

and [E] is a diagonal matrix in which each diagonal element is 1 except the first and last elements, which are $\frac{1}{2}$.

The stresses associated with the displacement given by equations (3) are

$$\tau_{xz}^{s\pm} = \hat{i}\mu \sum_{n=0}^{N}{}' k_n D_n^{\pm} \cos\beta_n y \tag{25}$$

where τ_{xz}^{s-} acts on R_1^- along the boundary AB and τ_{xz}^{s+} acts on R_1^+ along the boundary CD. In order to construct the desired boundary conditions we approximate the stresses of equation (25) by piecewise-uniform stresses of the type shown in Fig. 2. This means that these stresses are approximated by

$$\tau_{xz_j}^{s\pm} = i\mu \sum_{n=0}^{N} k_n D_n^{\pm} \cos\beta_n y_j \,, \quad \frac{h}{N}\left(j - \frac{1}{2}\right) \leq y \leq \frac{h}{N}\left(j + \frac{1}{2}\right) \tag{26}$$

These can be integrated over the interval to give the equivalent nodal line forces associated with the scattered field. Near the surface nodes A, S, C and D (Fig. 2) the stresses represented by dotted lines indicate that the node is subjected to a nodal force of half the value obtained from the stress used in the approximation. The nodal forces acting on R_2 due to the scattered field are, therefore, given by the expressions

$$\begin{aligned} F_j^{s\pm} &= -\frac{h}{N}\tau_{xz_j}^{s\pm} \,, \quad j \neq 0, N \\ F_j^{s\pm} &= -\frac{h}{2N}\tau_{xz_j}^{s\pm} \,, \quad j = 0, N \end{aligned} \tag{27}$$

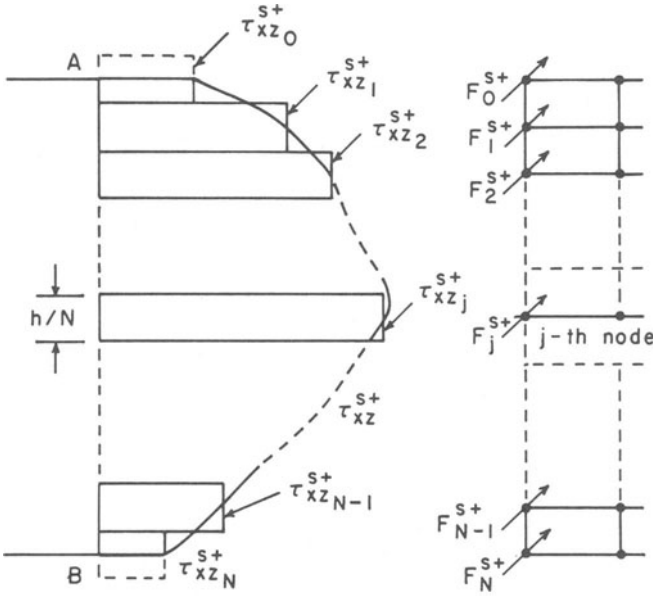

Fig. 2. Piecewise-uniform stress approximation.

This with expression (26) can be used to construct the matrix relation

$$\{F^{s\pm}\} = \frac{-\hat{i}\mu h}{N} [E][V][H] \{D^{\pm}\} \tag{28}$$

in which $\{F^{s\pm}\}$ denotes the column vectors containing the nodal forces $F_j^{s\pm}$. Also in (28) [H] denotes a diagonal matrix with the diagonal elements k_n, n = 0, ---, N. Substitution of expression (24) for $\{D^{\pm}\}$ into equation (28) leads to

$$\{F^{s\pm}\} = \frac{-2\hat{i}\mu h}{N^2} [E][V][H][E][V][E] \{w^{s\pm}\} \tag{29}$$

Expression (29) can be written in the compact form

$$\{F^{s\pm}\} = [Q] \{w^{s\pm}\} \tag{30}$$

where $[Q] = \frac{-2\hat{i}\mu h}{N^2} [E][V][H][E][V][E]$ is an (N+1) x (N+1) symmetric matrix.

The incident mode propagates in the direction of the scattered wave in R_1^+ and in a direction opposite to that of the scattered wave in R_1^-. This leads to the relations

$$\{F^{i\pm}\} = \pm [Q] \{w^{i\pm}\} \tag{31}$$

Here $\{F^{i\pm}\}$ represents the column vectors of the nodal forces associated with the incident mode.

The boundary forces of equation (17) can now be written as

$$\{F^{\pm}\} = \{F^{i\pm}\} + \{F^{s\pm}\} \tag{32}$$

Also, at the boundaries the nodal displacements can be related according to equation (1) by

$$\{w^{s\pm}\} = \{w^{\pm}\} - \{w^{i\pm}\} \tag{33}$$

in which $\{w^{\pm}\}$ denotes the column vectors of the nodal values of the total field. Substituting equations (30) and (31) into equation (32) and using relation (33) in the resulting expression, it is found that

$$\{F^{+}\} = [Q]\ \{w^{+}\} \tag{34a}$$

$$\{F^{-}\} = [Q]\ \{w^{-}\} - 2\ [Q]\ \{w^{i-}\} \tag{34b}$$

This completes the derivation of the boundary conditions associated with equation (16). After the substitution of equations (34) into equation (16) the terms $[Q]\{w^{-}\}$ and $[Q]\{w^{+}\}$ can be transferred to the left-hand side of the equation. These terms are then transformed to a global form and incorporated in the structure of the equation to obtain the relation

$$[S^{*}]\{w\} = \{F^{*}\} \tag{35}$$

where $[S^{*}]$ is a symmetric complex matrix and $\{F^{*}\}$ is a column vector, whose components are given by

$$F_i^{*} = \begin{cases} -2 \sum_{j=0}^{N} Q_{ij}\ w_j^{i-} & \text{if } i \text{ denotes a node along AB,} \\ 0 & \text{if } i \text{ denotes an inner or a surface node or a node along CD.} \end{cases} \tag{36}$$

In (36), Q_{ij} denotes the elements of the matrix $[Q]$ and w_j^{i-} denotes the j-th component of the column vector $\{w^{i-}\}$.

The problem is now reduced to solving equation (35) for the nodal values of the total field w. Equations (33) can then be used to obtain at the boundaries the nodal values of w^{s}. The amplitudes of the scattered modes are then computed from equations (24).

Before proceeding further a justification is needed of the assumptions made in the derivation of equation (29). To this aim the equation was written in the form (30). The symmetry of the matrix $[Q]$ implies that the assumptions made resulted in reciprocal force-displacement relations along the boundaries of the mesh. Reciprocity in this sense is an essential feature of the continuous system associated with the problem. Another feature which must be preserved concerns the rate of energy transmission per unit width of the mesh boundaries AB and CD. Appendix A presents the proof that the rates of energy transmission through these boundaries by the discrete systems of equations (30) are identical with the rates of energy transmission through the corresponding boundaries of the adjacent continuous regions. Finally, the model is tested for the satisfaction of the field-reciprocity relations in $R_1^{\pm}$. It is shown in Appendix B that the continuous and the discrete systems in this problem yield identical reciprocity relations.

III. SCATTERING BY A SURFACE CRACK

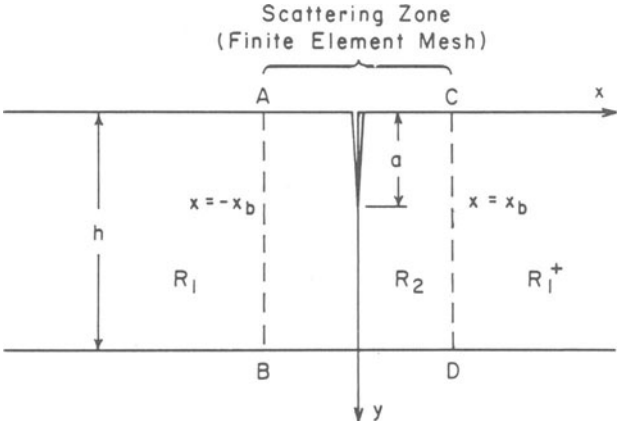

Fig. 3. Plate with a normal crack.

In this section the solution for a normal edge crack is presented. The crack is modeled by an infinitesimally thin notch $0 \leqq y \leqq a$, $x = 0$. In order to use the technique presented in this paper the region $-x_b \leqq x \leqq x_b$ is replaced by a finite element mesh, as shown in Fig. 3. The crack tip singularity is modeled by dividing the area around the crack tip into eight triangular shaped singularity elements[18]. These are surrounded by eight trapezoidal shaped transition elements[19]. The rest of the mesh is composed of rectangular four-noded isoparametric elements. Some of these are collapsed into triangular elements along the vertical sides of the transition elements, as illustrated in Fig. 4. This is done to increase the number of modes used in the analysis without increasing the number of the transition and singularity elements. The singularity and transition elements are generated from six-noded parent elements. All the shape functions used in conjunction with the elements of the mesh are polynomials of the Lagrangian type.

Three incident modes ($m = 0, 1, 2$) are considered here. Following the notation of Ref. 13, the solution in R_1 is expressed in

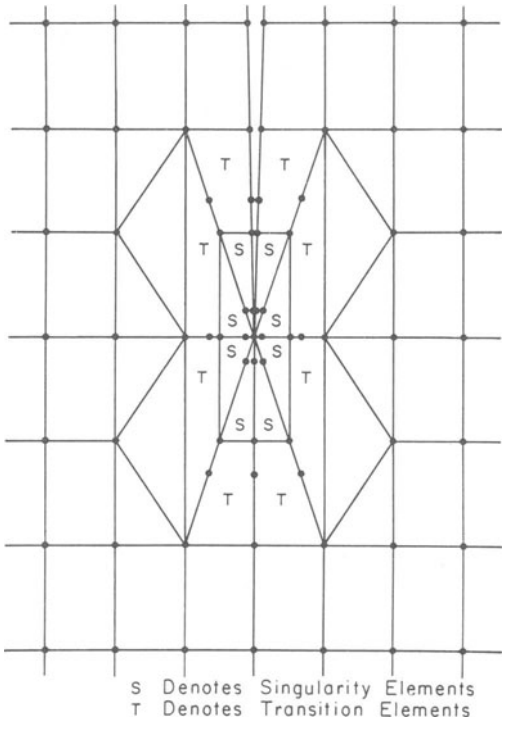

Fig. 4. Finite elements near the crack tip.

terms of reflected and transmitted fields. These fields are constructed by the superposition of the incident and the scattered modes. With the aid of equations (2) and (3) this leads to

$$w^{rfl} = \sum_{n=0}^{N} B_n \cos\beta_n y \, e^{-\hat{i}k_n x}, \quad x \leqq -x_b \tag{37}$$

and

$$w^{tr} = A_m \cos\beta_m y \, e^{\hat{i}k_m y} + \sum_{n=0}^{N} C_n \cos\beta_n y \, e^{\hat{i}k_n x}, \quad x \geqq x_b \tag{38}$$

Once B_n and C_n are obtained by the method outlined in section II equations (37) and (38) can be used to express the fields in $x < 0$ and $x > 0$ respectively. Division of equations (37) and (38) by A_m gives

$$R_{mn} = \frac{B_n}{A_m} \tag{39a}$$

$$T_{mn} = \frac{C_n}{A_m}, \; n \neq m, \; T_{mm} = 1 + \frac{C_m}{A_m} \tag{39b}$$

where R_{mn} and T_{mn} are the conversion coefficients for the reflected and transmitted waves, respectively. The coefficients R_{mm} and T_{mm} are the reflection and transmission coefficients for the m-th incident mode. It can be shown[13] that

$$R_{mn} = - T_{mn} \ , \ 1 - R_{mm} = T_{mm} \tag{40}$$

Also it was shown in Ref. 13 that

$$K_m R_{nm} = K_n R_{mn} \ , \ K_m R_{0m} = 2 K_s R_{m0}, \ m, \ n \neq 0 \tag{41}$$

The derivation of (41) is also reproduced in Appendix B. Another important concept is the principle of conservation of energy. This states that

$$I^{inc} = \sum_{n=0}^{N_p} (I_n^{tr} + I_n^{rfl}) \ . \tag{42}$$

where I^{inc} is the energy flux transported by the incident mode through the plane $x = 0$. Also in (42) I_n^{tr} and I_n^{rfl} represent the energy fluxes transported in the n-th transmitted and reflected modes through the cross-section of the plate at $x = 0$. The fluxes in equation (42) are obtained from the equation

$$I_n = - \frac{1}{2} \int_0^h R_e \, (\bar{\tau}_{xz_n} \dot{w}_n) \, dy = \begin{cases} - \frac{h}{4} \mu \omega k_n |A_n|^2, & n \neq 0 \\ \\ - \frac{h}{2} \mu \omega k_s |A_0|^2, & n = 0 \end{cases} \tag{43}$$

In (43) A_n represents the amplitude of the mode transporting the energy flux I_n. τ_{xz_n} and w_n are the stress and displacement associated with the mode under consideration. The overbar and the overdot in (43) denote the complex conjugate and the time derivative respectively. The approach taken in this paper involves a finite element approximation and uses truncated Fourier series in expressing the solution in the uniform regions of the plate. To assess the accuracy of the technique the error involved in the analysis can be estimated by the derivation from equation (42). This leads to the expression

$$\varepsilon = [\ I^{inc} - \sum_{n=0}^{NP} (I_n^{tr} + I_n^{rfl}) \ ] \ / \ I^{inc} \tag{44}$$

where ε denotes the relative error in the computation of the input energy flux I^{inc} from the reflected and transmitted energies.

IV. RESULTS AND DISCUSSION

In the present section, numerical results are presented for R_{mn}. In the example under consideration 21 terms in the Fourier series have been taken. This requires the use of 21 equally-spaced nodes along each of the vertical boundaries of the mesh. The mesh is automatically generated with arbitrary crack length in the range $0.1 \leqq \frac{a}{h} \leqq 0.9$ and a crack length increment of $\frac{a}{h} = 0.05$. It may be noted that this led to a number of nodes ranging from 211 to 227 depending on the crack length. Accordingly, the number of nodes on the crack face ranges from 9 to 41. To simplify the automatic generation of the mesh the elements are taken to be of equal heights and widths. Consequently, the number of modes used fixes the height of each element at 0.05h. The width of each element was taken to be 0.02h. The overall width of the mesh was taken to be $2x_b = 0.16$. With the mesh described above the error in the present calculations was found to lie within $|\varepsilon| \leqq 2\%$, where ε is given by equation (44). Fixing the number of modes at twenty-one, the maximum element width required to ensure convergence of the method was found to be one-tenth of the minimum wave length. In terms of the dimensionless frequency this can be written as $\frac{\pi}{5k_s h}$. All the results in the range of parameters reported here were found to be in agreement with relations (40) and (41) with negligible error.

The example being investigated was studied for the zeroth, first and second incident modes. The results are presented in terms of the reflection coefficients R_{mm} and the conversion coefficients for the reflected modes $(R_{mn},\ m < n \leqq N_p)$ of orders higher than m, where m is the order of the incident mode and N_p is the number of propagating modes. The conversion coefficients for the reflected modes of orders less than m can be computed from the reciprocity relations (41). The conversion coefficients for the transmitted modes and the transmission coefficients can then be obtained from equations (40).

In Figures 5 and 6 the moduli and arguments of the coefficients $R_{0n},\ 0 \leqq n \leqq N_p$ are plotted versus the normalized crack length $\frac{a}{h}$ for the dimensionless frequencies $k_s h = 9$ and 18. These are the coefficients associated with the zeroth incident mode. In Fig. 5 the results are compared with those of Ref. 3 which were obtained by an approximate variational method. It is seen that in the range of small crack lengths the results are in good agreement. The variational solution[3] deviates from our solution when a/h exceeds a value of 0.4. Next, the coefficients associated with the first incident mode $(R_{1n},\ 1 \leqq n \leqq N_p)$ are plotted in Figures 7 and 8 for the frequencies $k_s h = 9$ and 18. Figures 9 and 10 show the results for the incident second mode for the frequencies $k_s h = 9$ and 18. The variations of the coefficients $R_{0n},\ 0 \leqq n \leqq 5$, with the frequency $k_s h$ for the crack lengths $\frac{a}{h} = 0.3,\ 0.5$ and 0.9 are

variations of the coefficients R_{1n}, $1 \leqq n \leqq 5$, with the frequency $k_s h$ for the crack lengths $\frac{a}{h} = 0.3$, 0.5 and 0.9. In Figures 11-16, the dotted portions of the curves indicate non-propagating modes. The solid lines are for the range of frequencies for propagating modes. The abrupt variations at the critical frequencies $k_s h = n$ (n = 1, 2, ---) in Figures 11-16 are due to the inception of new propagating modes which causes a sudden change in the distribution of energy in the spectra of the reflected and transmitted waves. Near the critical frequencies the phases also suffer abrupt changes and for large cracks ($a/h \to 1$) are very sensitive to changes in $k_s h$. This is indicated by dashed lines in Figures 13 and 16. All the results presented in this paper agree closely with the figures of Ref. 13. However, no comparison is made here because of the unavailability of the numerical results.

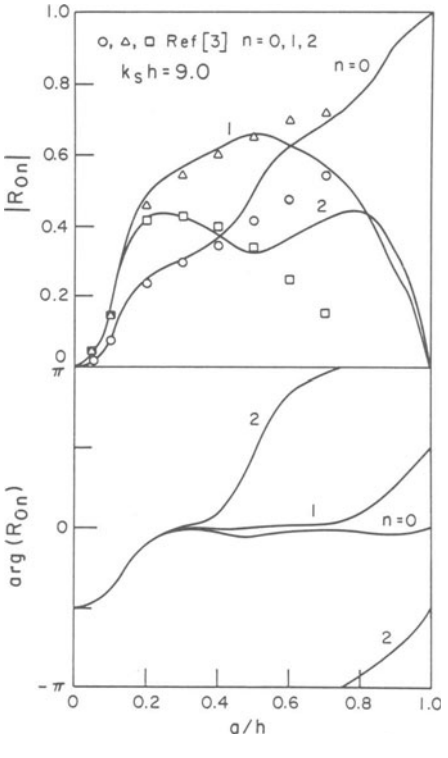

Fig. 5. R_{0n} vs. normalized crack length for a dimensionless

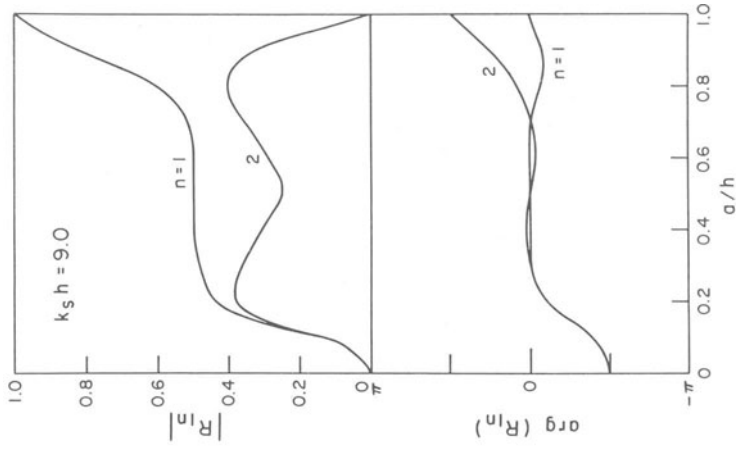

Fig. 7. R_{ln} vs. normalized crack length for a dimensionless frequency of 9.0.

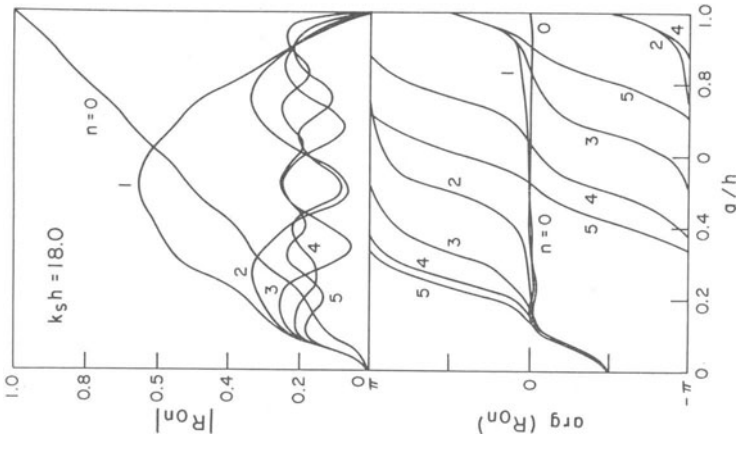

g. 6. R_{on} vs. normalized crack length for a dimensionless frequency of 18.

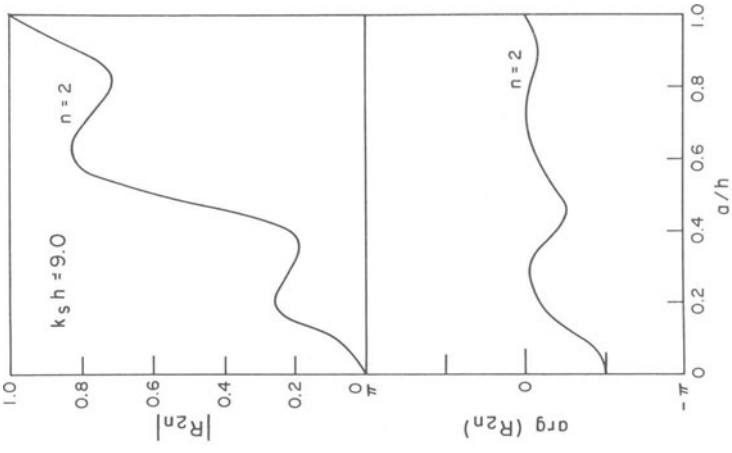

Fig. 9. R_{2n} vs. normalized crack length for a dimensionless frequency of 9.0.

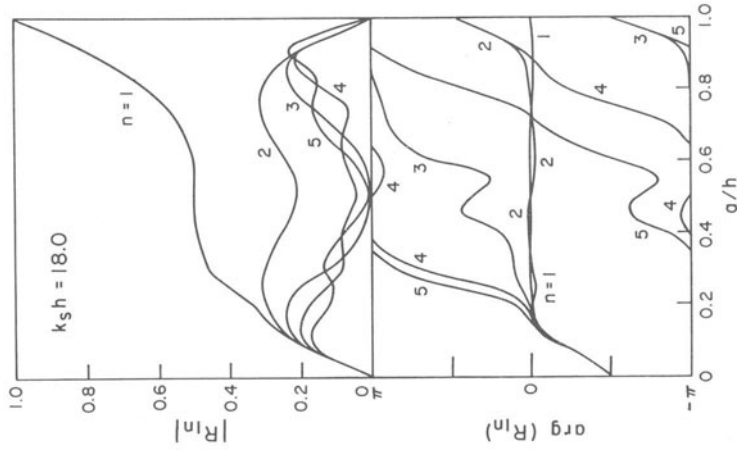

Fig. 8. R_{1n} vs. normalized crack length for a dimensionless frequency of 18.

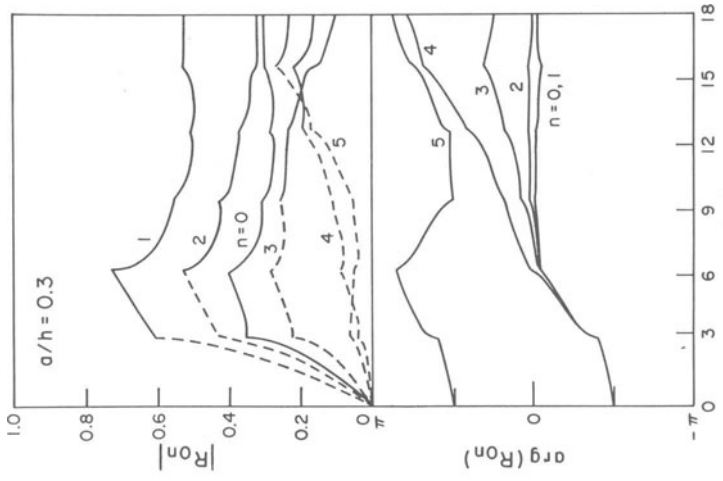

Fig. 11. R_{0n} vs. dimensionless frequency for a normalized crack length of 0.3.

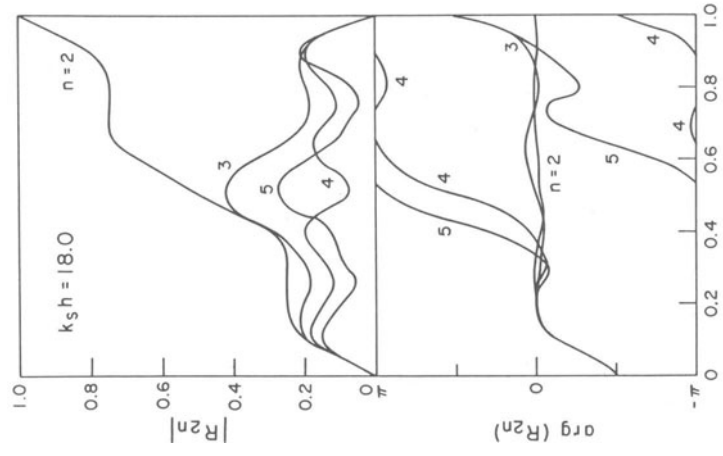

Fig. 10. R_{2n} vs. normalized crack length for a dimensionless frequency of 18.

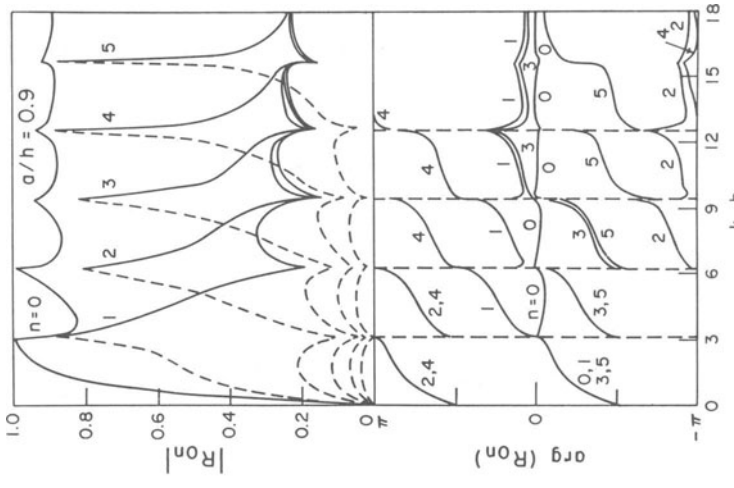

Fig. 13. R_{On} vs. dimensionless frequency for a normalized crack length of 0.9.

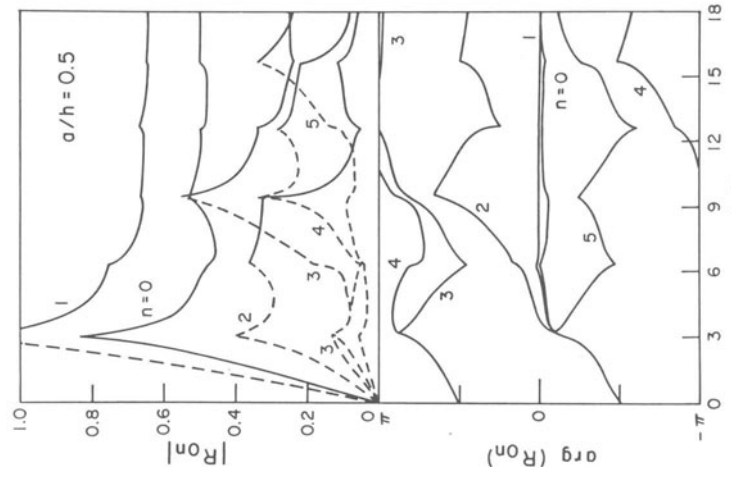

ig. 12. R_{On} vs. dimensionless frequency for a normalized crack length of 0.5.

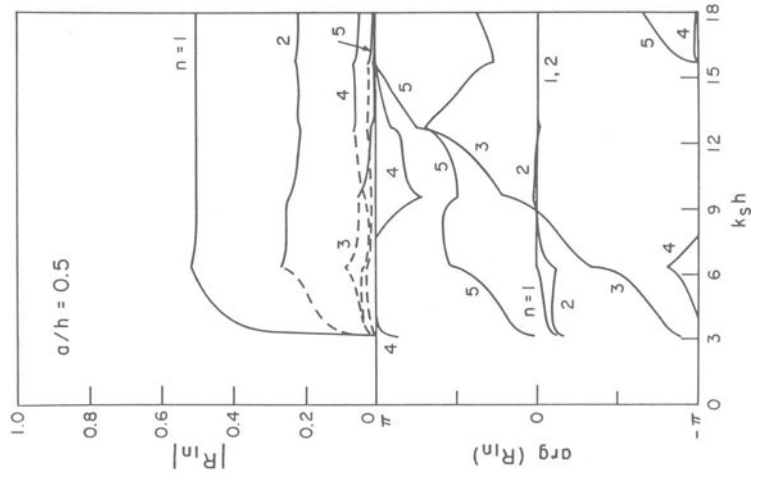

Fig. 15. R_{ln} vs. dimensionless frequency for a normalized crack length of 0.5.

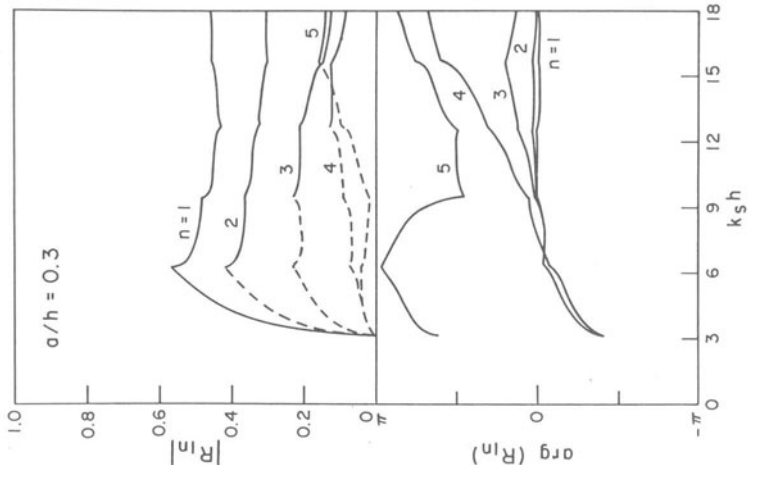

Fig. 14. R_{ln} vs. dimensionless frequency for a normalized crack length of 0.3.

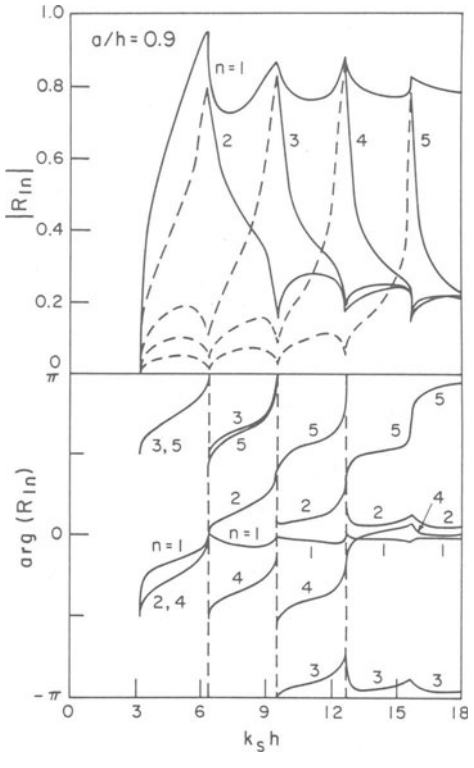

Fig. 16. R_{1n} vs. dimensionless frequency for a normalized crack length of 0.9.

V. CONCLUSION

A technique has been presented for studying the diffraction of horizonatally polarized shear (SH) waves in plates. The technique replaces the finite region containing the scatterers by finite elements. In the exterior regions the field is written as a modal sum. Continuity conditions at the boundary between the interior and exterior regions of the plate are then obtained with the aid of the discrete Fourier analysis. An important feature of the boundary forces obtained in this model is that they satisfy the reciprocity and the energy flux relations. The method is used to study diffraction of SH waves by a normal surface crack in a plate. The numerical results presented here agree well with other available results for the zeroth, first and second incident modes. The advantage of

the method is that it can be used to study diffraction of SH waves by cracks in anisotropic elastic weldments.

ACKNOWLEDGEMENTS

The work reported here was supported in part by a grant (CME-7824179) from the National Science Foundation. The first author is also grateful to the government of Saudi Arabia for granting a scholarship for graduate studies.

Appendix A. ENERGY TRANSMISSION THROUGH THE MESH BOUNDARIES

In this appendix, an expression for the energy flux across the mesh boundaries (AB and CD) is derived. The energy flux associated with the n-th propagating scattered mode through the boundaries AB and CD are denoted by I_n^- and I_n^+ respectively. These are given by the expressions

$$I_n^{\pm} = \frac{1}{2} \mathrm{Re} \left(\overline{\{F_n^{s\pm}\}}^T \{\dot{w}_n^{s\pm}\} \right), \quad n \leq N_p \tag{A1}$$

in which the overbar denotes the complex conjugate and $\{\dot{w}_n^{s\pm}\} = -i\omega \{w_n^{s\pm}\}$. The column vectors $w_n^{s\pm}$ and $F_n^{s\pm}$ represent the nodal displacements and line forces, at the boundaries, due to the n-th scattered mode. To obtain these vectors equations (23) and (28) are used with $D_n^{\pm}$ being the only non-zero components of $\{D^{\pm}\}$. Next, equation (24) is substituted into equation (23) to obtain the relation

$$\frac{2}{N} [E][V][E][V] = [I]$$

or

$$[V][E][V] = \frac{N}{2} [E]^{-1} \tag{A2}$$

where $[I]$ is the identity matrix.

Now the substitution of the results of equations (23) and (28) into equation (A1) and the use of relation (A2) results in

$$I_n^{\pm} = \begin{cases} -\frac{h}{4} \mu\omega k_n |D_n^{\pm}|^2, & n \neq 0 \\ -\frac{h}{2} \mu\omega k_s |D_0^{\pm}|^2, & n = 0 \end{cases} \tag{A3}$$

The expressions in (A3) are identical with those of the corresponding continuous system which are available elsewhere.[13] Similar expressions can be found for the energy transmitted with the incident mode.

Appendix B. FIELD-RECIPROCITY

In this appendix, the field-reciprocity relation of the plate is obtained and the consistency of the model presented in the paper is established. By definition, the field-reciprocity relation is a relation between two of the field quantities associated with two non-identical elastodynamic states that can be present in the plate. The two elastodynamic states can be written as

$$w_A = \cos\beta_m y\, e^{\hat{i}k_m x} + \sum_{\ell=0}^{N} R_{m\ell}\cos\beta_\ell y\, e^{-\hat{i}k_\ell x}, \quad x \leqq -x_\ell$$

$$w_B = \cos\beta_n y\, e^{\hat{i}k_n x} + \sum_{\ell=0}^{N} R_{n\ell}\cos\beta_\ell y\, e^{-\hat{i}k_\ell x}, \quad x \leqq -x_\ell \tag{B1}$$

In (B1) $R_{m\ell}$ and $R_{n\ell}$ are the reflection coefficient defined in (39). The state A is the superposition of an m-th incident mode with unit amplitude and the sum of the modes reflected from the scattering zone. The state B is analogous to A and is generated as a result of incidence of the n-th mode. Each of the states A and B satisfies the Helmholtz equation in R_1 (Fig. 1) and can be used in a two-dimensional Green's formula in the domain bounded by the surfaces of the plate and the two cross sections $x = x_1$ and $x = x_2$, where $x_1, x_2 \leqq -x_\ell$. This with the boundary conditions on the surfaces of the plate results in

$$\int_0^h \left(w_A \frac{\partial w_B}{\partial x} - w_B \frac{\partial w_A}{\partial x}\right)_{x=x_1} + \int_0^h \left(w_A \frac{\partial w_B}{\partial x} - w_B \frac{\partial w_A}{\partial x}\right)_{x=x_2} dy = 0 \tag{B2}$$

with x_1 and x_2 being chosen arbitrarily. This implies that each of the integrals is independent of x and is equal to zero. Thus

$$\int_0^h \left(w_A \frac{\partial w_B}{\partial x} - w_B \frac{\partial w_A}{\partial x}\right)_{x=x^*} dy = 0 \tag{B3}$$

Expression (B3) represents the general form of the reciprocity relation in the plate. It relates the displacements and their x-derivatives for the states A and B. Upon substituting (B1) into (B3) and using the orthogonality of the trigonometric functions

the relations (41) are obtained. These are $K_m R_{nm} = k_n R_{mn}$, $K_m R_{0m} = 2K_s R_{m0}$, m, n $\neq 0$.

If x^* in equation (B3) is chosen to represent the boundary AB ($x^* = -x_\ell$) of the mesh then the integrand in equation (B3) is replaced by an approximation similar to that of Fig. 2. This yields the relations

$$\int_0^h w_A \frac{\partial w_B}{\partial x} = \frac{h}{N} \sum_{j=0}^{N}{}' (w_A)_j \left(\frac{\partial w_B}{\partial x} \right)_j$$

and (B4)

$$\int_0^h w_B \frac{\partial w_A}{\partial x} = \frac{h}{N} \sum_{j=0}^{N}{}' (w_B)_j \left(\frac{\partial w_A}{\partial x} \right)_j$$

Here the subscript j denotes the value at the j-th node and the symbol $\sum'$ means that both the first and last terms in the summation must be multiplied by $\frac{1}{2}$. Now recalling the orthogonality relation (20) for the discrete Fourier analysis (B4) and using equations (B1) and (B4) expressions identical to those of (41) are obtained. From the foregoing it is concluded that the approximation used in the analysis results in the correct field-reciprocity.

REFERENCES

1. C. M. Fortunko, in Proc. 1980 Ultrasonics Symposium, B. R. McAvoy, ed., IEEE, New York (1980) 862-867.
2. C. M. Fortunko and R. E. Schramm, in Proc. of Fitness-for-purpose in Welded Construction Conf., R. W. Nichols, ed., The Welding Institute, Cambridge, England (1981) 20.
3. C. M. Fortunko, R. B. King, and M. Tan, J. Appl. Phys. 53:3450 (1982).
4. S. F. Stone, M. L. Ghosh, and A. K. Mal, J. Appl. Mech. 47:359 (1980).
5. D. A. Mendelsohn, J. D. Achenbach, and L. M. Keer, Wave Motion 2:277 (1980).
6. J. D. Achenbach and R. J. Brind, J. Sound Vib. 76:43 (1981).
7. R. J. Brind and J. D. Achenbach, J. Sound Vib. 78:555 (1981).
8. S. K. Datta, J. Appl. Mech. 46:101 (1979).
9. S. K. Datta, A. H. Shah, and C. M. Fortunko, J. Appl. Phys. 53:2895 (1982).
10. A. H. Shah, K. C. Wong, and S. K. Datta, Earthquake Eng. Struct. Dyn. (in press).
11. S. K. Datta and A. H. Shah, Wave Motion (in press).
12. J. Lysmer and G. Waas, J. Eng. Mech. Div. 98:85 (1972).
13. N. N. Egorov and A. V. Kharitonov, Sov. Phys. Acoust. 25(1):34 (1979).

14. O. C. Zienkiewicz, "Finite Element Method," McGraw-Hill, London (1977).
15. R. D. Cook, "Concepts and Applications of Finite Element Analysis," John Wiley and Sons, New York (1974).
16. F. S. Acton, "Numerical Methods that Work," Harper and Row, New York (1970).
17. G. Dahlquist, "Numerical Methods," Prentice-Hall, London (1969).
18. R. S. Barsoum, Int. J. Num. Meth. Eng. 12:31 (1978).
19. P. P. Lynn and A. R. Ingraffia, Int. J. Num. Meth. Eng. 12:31 (1978).

DISCUSSION

J.D. Achenbach (Northwestern University): Did you solve this crack problem by putting a finer element mesh around the cracks and matching them?

Z. Abduljabbar (University of Colorado): Exactly.

J.D. Achenbach: I believe that there are other ways--and in fact, I believe other investigators are solving this problem.

Z. Abduljabbar: Yes. This problem has actually been solved with a different method.

J.D. Achenbach: I believe by the T-matrix method, and also by reducing it to a single integral equation.

Z. Abduljabbar: Exactly, yes. The power of this method is in its applicability to cases where you have an an anisotropy or geometries that are difficult to handle with different methods. The only problem with it is that it is too expensive.